AIMS Biophysics

AIMS Biophysics, 7(4): 380–392.
DOI: 10.3934/biophy.2020026
Received: 11 July 2020
Accepted: 20 September 2020
Published: 25 September 2020

http://www.aimspress.com/journal/biophysics

Research article

A molecular modeling study of novel aldose reductase (AR) inhibitors

Auwal Muhammad[1], Kanikar Muangchoo[2,*], Ibrahim A. Muhammad[3], Ya'u S. Ajingi[4], Aliyu M. Bello[5], Ibrahim Y. Muhammad[1], Tasi'u A. Mika'il[3] and Rakiya Aliyu[1]

[1] Department of Physics, Faculty of Science, Kano University of Science and Technology (KUST), Wudil, Kano, Nigeria
[2] Faculty of Science and Technology, Rajamangala University of Technology Phranakhon (RMUTP), Bang Sue, Bangkok, Thailand
[3] Department of Biochemistry, Faculty of Science, Kano University of Science and Technology (KUST), Wudil, Kano, Nigeria
[4] Department of Biology, Faculty of Science, Kano University of Science and Technology (KUST), Wudil, Nigeria
[5] Department of Biochemistry, Faculty of Basic Medical Sciences, Bayero University Kano (BUK), Kano, Nigeria

* **Correspondence:** Email: kanikar.m@rmutp.ac.th; Tel: +66636517879.

Abstract: Aldose reductase (AR) is an enzyme of the polyol pathway implicated in long-term effect of diabetes mellitus. The development of new molecules as drugs for the inhibition of this enzyme is a growing area of research. Several *in vivo* and *in vitro* studies have been carried out to test the inhibitory effect of many organic compounds against AR, but the results have been limited due to their weak pharmacokinetic parameters and safety profile. In this study, molecular docking and molecular dynamics (MD) simulation were performed to establish the inhibitory effect of two critical bioactive compounds (astaxanthin and zeaxanthin) that were affirmed to be safe and powerful antioxidants. Docking studies revealed that both astaxanthin and zeaxanthin displays good binding affinity and inhibition to AR with binding energies of −5.88 kcal/mol and −5.63 kcal/mol, respectively. In contrast to epalrestat; the standard inhibitor having a binding energy of −5.62 kcal/mol. Amino acid residue analysis has shown that both compounds, including the standard inhibitor, bind to the same site due to their common interaction with Trp20 and Tyr48 at AR catalytic site. To complement molecular docking results, we performed MD simulations. The results show that the binding energies of the standard inhibitor, astaxanthin, and zeaxanthin are −134.3486 kJ/mol, −186.271 kJ/mol, and −123.557 kJ/mol, respectively. In both cases, astaxanthin displays better inhibition to AR followed by the standard inhibitor and zeaxanthin.

Keywords: aldose reductase; bioactive compounds; binding energy; molecular docking; molecular dynamics

1. Introduction

Diabetes is a group of metabolic disorders associated with an increase in blood sugar (hyperglycemia) due to either inability of cells to respond to the action of insulin (a hormone that regulates the amount of blood sugar) or impairment in insulin secretion. Increased glucose level results in symptoms such as polyuria, polyphagia, and polydipsia. There are many complications associated with uncontrolled diabetes and are categorized into acute and chronic. Diabetic ketoacidosis and non-ketotic hyperosmotic coma are examples of some of the acute implications. In contrast, cardiovascular diseases, foot ulcers, renal damage (diabetic nephropathy), and eye damage (diabetic retinopathy) are the result of chronic effects of diabetes, inflicting various tissues and organ damage [1]. Diabetic retinopathy was found to be the most important cause of vision impairment in the western world, and cataract has been listed among the three causes of vision impairment across the globe. Diabetes was found to be one of the most critical risk factors in retinopathy and cataracts [2]. A cataract is the cloudiness of the eye lens, contributing to about 40% of all blindness. More than 17 million people had vision impairment due to cataracts, with 28000 new cases daily [3]. Cataract caused by diabetes is associated with an elevated level of sorbitol in the eyes' retina due to increased aldose reductase activity. Aldose reductase (AR), otherwise known as alditol: NADP+ 1-oxidoreductase with enzyme classification (EC) number 1.1.1.21, is an NADPH dependent enzyme implicated in the long-term effect of diabetes like diabetic neuropathy, diabetic nephropathy, diabetic retinopathy, and cataractogenesis [2].

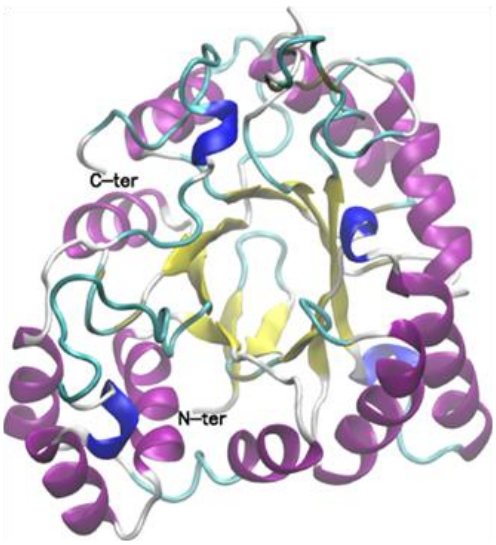

Figure 1. Structure of aldose reductase retrieved from the PDB database with ID: 1XGD and 2.1 Å resolution.

The use of natural bioactive compounds such as flavones, flavonoids and coumarins obtained from photosynthetic systems, for the inhibition of aldose reductase is recently growing. Several research have been conducted to study aldose reductase inhibition using either synthetic or natural inhibitors to minimize the incidence of the chronic effects of diabetes, including blindness associated

with cataract [1]. Many compounds such as epalrestat, sorbinil, tolrestat, and fidarestat (Figure 2) display good inhibitory activity against aldose reductase *in vivo* using animal models. However, most of them were later withdrawn from the market due to their side effects and non-selectivity for the enzymes that share sequence homology to aldose reductase; for example, aldehyde reductase has 51% amino acid homology to aldose reductase. However, only epalrestat (a synthetic aldose reductase inhibitor) was found to be successful in a clinical trial and commercially available to treat diabetic neuropathy in Japan and other parts of the world [4]. Because of the increasing number of diabetic cataract cases worldwide, there is a need for an alternatives and more effective AR inhibitors for the control of diabetic cataracts and other long-term diabetes effects.

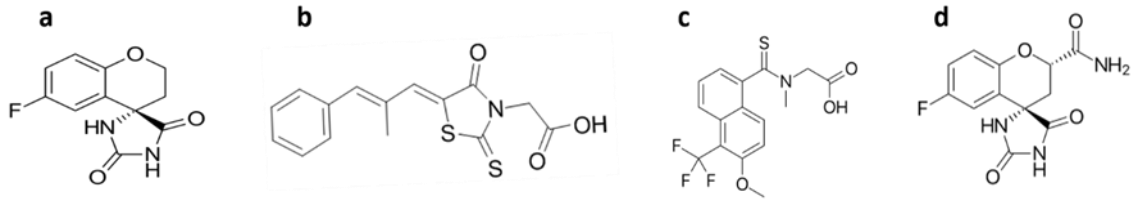

Figure 2. Some active aldose reductase inhibitors a) Sorbinil, b) Epalrestat, c) Tolrestat, d) Fidarestat.

Zeaxanthin and its structural isomer lutein are natural pigments that belong to xanthophyll carotenoids. They are found in dark-green leafy vegetables and egg-yolk. They are distributed in various tissues and form the principal part of the retina's eye lens and macula area. Many studies have indicated the potential benefit of xanthophyll in eye protection, decreased risk of cataracts, and age-related macular degeneration, breast, and lung cancer development, protection from stroke and cardiovascular diseases [5,6]. The mechanism of prevention of zeaxanthin cataractogenesis is attributable to its ability to absorb blue light and prevent oxidative stress [5].

Like zeaxanthin, astaxanthin belonged to xanthophyll carotenoids and was considered as a potent antioxidant capable of scavenging free radicals and exhibit anti-oxidative, anti-inflammatory, anti-apoptotic, and many other important pharmacological activities. It is an essential bioactive compound and a derivative of zeaxanthin and canthaxanthin containing ketone and hydroxyl functional groups. It is found in microalgae, yeast, trout, shrimp, and most of the red-colored aquatic life. Astaxanthin can be produced, employing both natural and chemical synthetic methods. *Haematococcus pluvialis* is one of the primary natural sources of astaxanthin. More than 50 researches have been carried out to explore astaxanthin's bioactivities, and it was established that astaxanthin display cardioprotective effect, improved eyesight, and anticancer activity, antidiabetic activity, skin protection, and many other activities. The antioxidant activity of astaxanthin was found to be due to polyene groups and multiple double bonds, and it can bind to the membrane to prevent lipid peroxidation. Its antioxidant activity is 65 times higher than ascorbic acid (vitamin C) and 50 times more potent than vitamin E, 11 times higher than beta carotene, and 2.7 times higher than lutein [7]. The potential effect of astaxanthin on metabolic cataract associated with type 1 diabetes has been investigated [8]. The authors found that astaxanthin could diminish the progression of cataract development in the eye lens of diabetic rats via its anti-oxidative stress activity. In a related study, astaxanthin was proved to be effective in preventing glucocorticoid-induced cataractogenesis in chick

embryo [9].

Albeit, there are reported *in silico* studies using molecular dynamics simulation and molecular docking that delineate the molecular interaction mechanism between aldose reductase and its inhibitors, but such investigations are limited. Although experimentally, aldose reductase has been reported to be inhibited by astaxanthin in *Psammomys obesus* [10]. Moreover, as far as we know, this is the first computational study of aldose reductase inhibitions explicitly using zeaxanthin and astaxanthin. It was also not established whether zeaxanthin and astaxanthin antioxidant activity could be related to the increase in NADPH (reduced nicotinamide adenine dinucleotide phosphate which indirectly participates in the elimination of free radicals) level through aldose reductase inhibition. In this study, we investigated *in silico* molecular interaction mechanism between zeaxanthin, astaxanthin, and aldose reductase to find binding conformations and possible inhibitory effect of zeaxanthin and astaxanthin to aldose reductase. Our study also compared the binding energy, inhibition constant, and other docking parameters of known aldose reductase inhibitor (Epalrestat) with zeaxanthin and astaxanthin bioinformatics tools.

1.1. Theory

Ligand binding energy corresponds to the energy released upon the formation of non-covalent binding interactions between an enzyme (E) and it is substrates (S) [11]. The interactions of enzymes with ligands are fundamental to both actions of numerous pharmaceutical compounds and a wide variety of biological processes. One of the essential characteristics of such interactions is the relationship between molecular structure and binding thermodynamics. It is a quantitative understanding of which would greatly benefit structure-based drug design [12]. The reversible process represents the formation of the complex, and the affinity of equilibrium association constant, K_a, is given as follows [13]:

$$\mathrm{E} + \mathrm{S} \leftrightarrow \mathrm{ES} \tag{1}$$

$$\mathrm{K_a} = \frac{[\mathrm{ES}]}{[\mathrm{E}][\mathrm{S}]} \tag{2}$$

At equilibrium, under conditions of constant pressure, the equilibrium constant can be related to the Gibbs free energy of binding (ΔG_{bind}) by the equation

$$\Delta \mathrm{G_{bind}} = -\mathrm{RTln}\mathrm{K_a} \tag{3}$$

R is gas constant with a value of $8.314\ \mathrm{JK^{-1}mol^{-1}}$, and T is the temperature in Kelvin. More negative values of $\Delta \mathrm{G_{bind}}$ reflect a more favorable reaction [14]. In thermodynamics, binding is governed by enthalpic and entropic components [13] given by

$$\Delta \mathrm{G_{bind}} = \Delta \mathrm{H} - \mathrm{T}\Delta \mathrm{S} \tag{4}$$

ΔG_{bind} is the binding free energy, ΔH is the enthalpy, ΔS is entropy, and T is the Kelvin scale's temperature. All the binding and free binding in biomolecular associations procedures are either driven from enthalpy (ΔH) or entropy (ΔS). The enthalpic component includes several types of non-covalent

interactions, such as van der Waals, electrostatic, hydrogen bonds, and halogen bonds. In contrast, the entropic components reflect the contribution to binding due to the system's flexibility or dynamics. The entropic component calculation is ignored in the current study because it is complicated, and algorithms are computationally very demanding [15].

2. Materials and methods

2.1. Ligands preparations

All the ligands (Epalrestat, astaxanthin, and zeaxanthin) were retrieved from the PubChem compounds database [16] with PubChem ID of 15490120, 5281224, and 5280899, respectively. The structure files were saved as sdf format. These ligands were then converted into three-dimensional 3D .pdb format with Avogadro software [17].

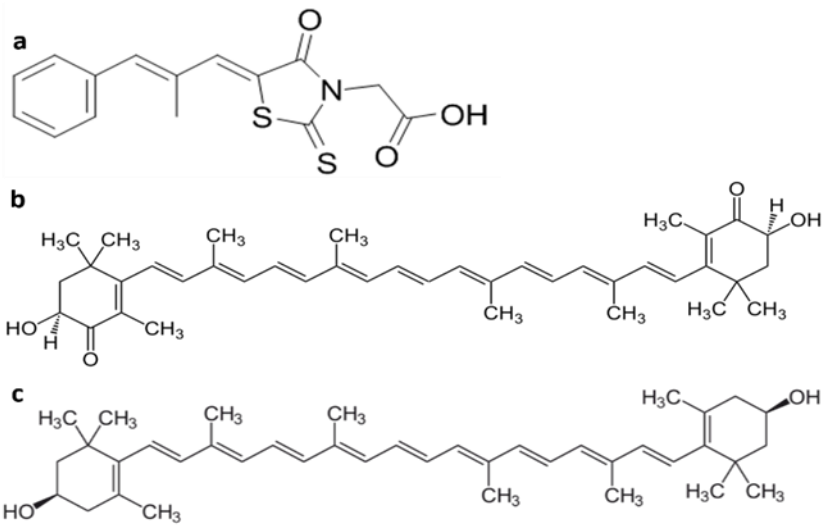

Figure 3. Molecular structures of the inhibitors used in this study: (a) Epalrestat, (b) Astaxanthin, and (c) Zeaxanthin.

2.2. Protein model preparations

The co-ordinate of aldose reductase with PDB ID: 1XGD [18] was retrieved from the protein data bank (https://www.rcsb.org/). Crystallographic water molecules were removed, and hydrogen atoms were added to the crystal structure with the help of the AutoDock Tool before docking. The protein structures were prepared by Autodock 4.2 software [19].

2.3. Molecular docking

The PDB files for both the targets were prepared using AutoDockTools (ADT). The ligand optimization was performed using Autodock 4.2 [19], Gasteiger charges were added, non-polar hydrogens were merged, and saved as PDBQT file. Atom charges, solvation parameters, and polar hydrogen were added to the protein receptor for docking simulation, and the file converted to the

PDBQT file. For calculation of docking interaction energy, the grid box was created and enclosed the protein molecules. The grid volume should be large enough to allow the ligand to rotate freely. The grid dimensions used were X = 126, Y = 126 and Z = 126. The autogrid, grid point spacing, was 0.492 Å. The parameters used to create such a grid were stored in a grid parameter file, grid.gpf. Parameters considered during docking experiments were Genetic Algorithm (GA) runs 10, population size 150, mutation rate 0.02, and crossover rate 0.8. Docking simulations were carried out to 2.5 million energy evaluations steps with a maximum of 270000 generations and stored in a dock parameter file, dock.dpf. Upon completion of the docking simulation, 10 docked conformations were produced. The lowest energy conformations were regarded as the best binding conformations between ligands and the receptor. The interactions analysis of the selected docked conformations was plotted with Ligplot+ [20].

2.4. Molecular dynamics (MD) simulations and analysis

Molecular dynamics (MD) simulations were performed with Gromacs 5.1.2 [21] using the GROMOS54A7 force field [22] for protein and solvated by the addition of TIP3P water molecules [23]. The starting conformation of each protein–inhibitor complex was taken from the molecular docking result of AutoDock. Force field parameters for each ligand were generated from the Automated Topology Builder (ATB) webserver [24] with the GROMOS54A7 force field. The box dimension created for each was 8 nm × 8 nm × 8 nm. Two Na^+ counterions were applied to neutralize the system and prevent the infinite charge from the periodic boundary condition implemented along with the Particle Mesh Ewald (PME) [25]. Each system then undergoes the minimization of energy using the steepest descent algorithm at 50,000 steps. Then, we equilibrated the systems with simulated annealing for a period of 1-ns, that linearly raised the temperature from 100 to 300 K at 1 atm, in an NPT ensemble with velocity-rescaling thermostat and Berendsen barostat [26], so that the solvent slowly changed to the liquid phase, allowing solute molecules to move with greater freedom. Eventually, each system underwent production MD for 50.0 ns with temperature and pressure of 300 K and 1 atm, respectively, under NPT ensemble with velocity-rescaling thermostat and Parrinello-Rahman barostat [27] to maintain temperature and pressure of the system close to reference values. After completing the simulations, water molecules were eliminated from the trajectories and translational and rotational motions, so only internal motions of protein-ligand complexes were analyzed. Visual Molecular Dynamics (VMD) [28] was used to visualize and analyze the molecular structures during simulation setup and MD trajectories analysis.

2.5. Binding free energy calculations

The binding free energy of protein-ligand was evaluated using Gromacs and the MM/PBSA technique developed by [29], in a relatively computationally-efficient manner [30]. The equation gives the binding free energy (ΔG):

$$\Delta G_{bind} = G_{comp} - G_{receptor} - G_{ligand} \tag{5}$$

Where G_{comp}, $G_{receptor}$, and G_{ligand} represent the energies of the complex, protein, and inhibitors, respectively. The free energy of these parameters is calculated as the sum of the following terms:

$$G_{bind} = E_{MM} + G_{sol} - TS \tag{6}$$

$$E_{MM} = E_{int} + E_{vdw} + E_{ele} \quad (7)$$

$$G_{sol} = G_{sol-elect} + G_{np} \quad (8)$$

Where E_{MM} represents molecular mechanics free energy in a vacuum, which is computed using classical force fields; G_{sol} is computed using the PBSA method; $G_{sol-elect}$ is computed using the PB method, and the G_{np} is computed by solvent accessible surface area (SASA). While employing a single trajectory approach, E_{int} is the internal energy that makes a negligible contribution to the binding energy and generally cancels out [15]. For implicit solvation, the dielectric constant of proteins and solvent was set to 4 and 80. The solvent-accessible surface area (SASA) model was used for the calculation of nonpolar solvation energy. We used the default values of surface tension of the solvent and SASA energy constant that were set to 0.0226778 kJ/(mol Å^2) and 3.84982 kJ/mol [31]. MM/PBSA calculations were performed for snapshots taken every 0.1 ns from the last 20 ns of each protein–inhibitor complex MD trajectories. Per energy residue contributions was also done to see the contribution of each amino acid residue to total binding free energy.

3. Results and discussions

3.1. Molecular docking results

Molecular docking is an *in-silico* approach that is used to predict binding conformations and binding potential of organic compounds (mostly small organic molecules) called ligands to a large organic compound otherwise called receptors [32]. Molecular docking studies of epalrestat, astaxanthin, and zeaxanthin were performed with aldose reductase to estimate the intermolecular energy, binding free energy, and inhibition constant (Table 1).

Table 1. Estimated the lowest binding energy of aldose reductase in complex with inhibitors obtained from molecular dockings. Predicted intermolecular energy and inhibition constants were also shown.

Inhibitors types	Intermolecular Energy (kcal/mol)	Binding Energy (kcal/mol)	Inhibition constants (uM)
Epalrestat	−7.41	−5.62	75.31
Astaxanthin	−9.46	−5.88	49.90
Zeaxanthin	−9.21	−5.63	74.71

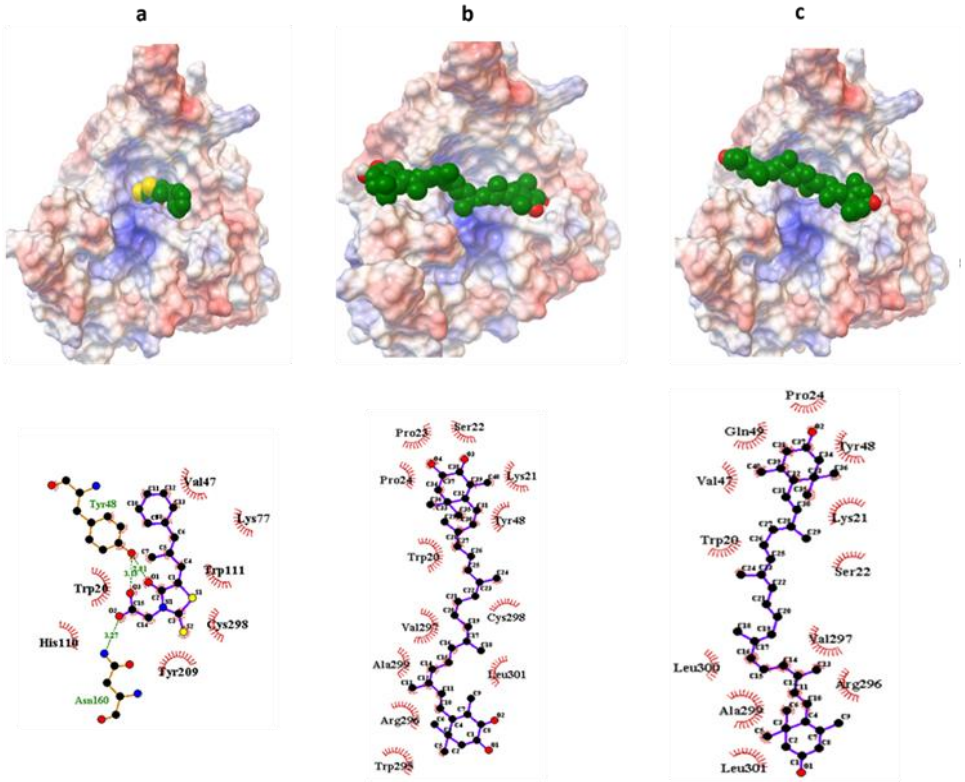

Figure 4. Docking structure of AR in complex with inhibitors (top) and Interaction details (bottom) produced by Ligplot+ a) Epalrestat, b) Astaxanthin, and c) Zeaxanthin.

All the hypothesized inhibitors showed good binding affinity and inhibition potential measured by the binding energy and inhibition constant. The binding energy (−5.62 kcal/mol) of the known inhibitor (epalrestat) was weaker than that of astaxanthin and zeaxanthin with binding energy −5.88 kcal/mol and −5.63 kcal/mol, respectively. The better binding energy of astaxanthin and zeaxanthin relative to epalrestat could be related to their hydrophobic interaction with various amino acid residues in AR's active site. Based on the binding energy and inhibition constant values obtained, we inferred that astaxanthin and zeaxanthin could inhibit AR better than the known inhibitor. The inhibition constant for epalrestat, astaxanthin, and zeaxanthin recorded were 75.31, 49.00, and 74.71 μM, respectively. The lower the inhibition constant, the stronger the binding affinity. Our result agrees with that of [33], who studied the inhibitory effect of some selected flavonoids (xanthotoxin and other flavonoids). They observed that epalrestat (used as reference standard inhibitor) could bind and inhibit AR with a binding energy of −5.59 kcal/mol and inhibition constant of 80.08 μM while xanthotoxin has −7.2 kcal/mol and 4.86 mM of binding energy and inhibition constant, respectively. Although xanthotoxin has higher binding energy than astaxanthin and zeaxanthin in our studies, its inhibition constant is very low, indicating that astaxanthin and zeaxanthin could better inhibit AR compared to xanthotoxin. To further establish whether astaxanthin and zeaxanthin bind to the same active site of AR where standard inhibitor bind, we studied the interaction of various conformations of compounds with AR. According to [34,35,36], the key active site amino acid residues are Tyr48, His110, Lys77, Trp111, Trp20, and Lys21. In our study, we observed that AR-epalrestat interaction was mediated by Trp20, Val47, Tyr48, Lys77, His110, Trp111, Asn160, Tyr209, and Cys298 amino acids residues

mostly via hydrophobic interactions with three hydrogen bonds formation via Tyr48 and Asn160 (Figure 4a [bottom]). Also Figure 4b (top) showed the docking structure of AR in complex with the Astaxanthin molecule. The amino acid residues that participated in the binding are Trp20, Lys21, Ser22, Pro23, Pro24, Tyr48, Trp295, Arg296, Val297, Cys298, Ala299, and Leu301 (Figure 4b [bottom]). In the docking structure of AR in complex with zeaxanthin molecule Figure 4c (top), the observed nature of the association between AR and zeaxanthin reveals Trp20, Lys21, Ser22, Pro24, Val47, Tyr48, Gln49, Arg296, Val297, Ala299, Leu300, and Leu301, as amino acids residues involved in the interactions as seen in Figure 4c (bottom). Based on this analysis, we reported that all the compounds bind to the AR active site due to the complementarity of the amino acids that participated in all the ligands' interactions with those in the AR active site.

3.2. MD simulations

To understand the nature of the association between AR and its inhibitors, MD simulations were performed to support the docking studies results further. Three MD simulation systems of 50 ns were prepared for the known inhibitor (epalrestat). Each of astaxanthin and zeaxanthin, respectively, in order to confirm the variation in the mobility of each of the inhibitors. The initial details of each system are summarized in Table 2.

Table 2. Detailed of three systems considered in MD Simulations.

System	Number of TIP3P water molecules	Number of Na^+ ions	System sizes (nm)
AR-Epalrestat	17705	2	8.38*8.38*8.38
AR-Astaxanthin	17693	2	8.38*8.38*8.38
AR-Zeaxanthin	17691	2	8.38*8.38*8.38

MD simulations results have shown that known inhibitors and compounds could bind to certain common amino acid residues of AR molecules, consistent with our docking results. The known inhibitor formed hydrogen bonds with Trp20 (76.62%), Tyr48 (25.87%), and Val47 (15.42%) of AR. However, it also established hydrophobic interactions with Lys21, Asp43, Gln49, Glu51, Trp79, Phe121, and Lys262. Most of these residues were also found in docking results as amino acid residues that participated in the interaction between AR and Epalrestat. Furthermore, Tyr48 formed a hydrogen bond with epalrestat in both docking and MD simulations. Astaxanthin established hydrogen bond interactions with Arg296 (15.42%), Trp111 (18.41%) and Leu300 (17.41%), and also hydrophobic interaction with Trp20, Lys21, Tyr48, Phe121, Trp219, Arg293, Ala299, Pro310 and Glu313Ala1. Zeaxanthin formed interactions with Lys21, Pro23, Pro24, Val47, Glu51, Trp79, Trp111, Glu120, Phe122, and Lys262. However, in comparison with known inhibitor and astaxanthin, the following common residues Trp20, Lys21, Tyr48, Phe21, and Ala299, were observed. Similarly, epalrestat and zeaxanthin shared the common residues of Lys21, Val47, Glu51, and Trp79.

3.3. MM/PBSA binding energy analysis

To investigate the detailed interactions between AR in complexes with inhibitors, MM/PBSA

analysis was performed over the last 20 ns of all MD simulations. Time-averaged total binding free energy and the contributions from van der Waals, electrostatics, polar and nonpolar solvation are presented in Table 3. The range of binding free energy of AR in complex with inhibitors was observed from −123.557 kJ/mol to −186.271 kJ/mol. The results showed that the average binding free energy for AR in complexes with known inhibitor, astaxanthin, and zeaxanthin was −134.755kJ/mol, −186.271kJ/mol, and −123.557 kJ/mol, respectively.

Table 3. MM/PBSA binding free energy of each complex. Contributions from van der Waals interactions, electrostatic interactions, polar and apolar solvation are also presented.

Inhibi –tors type	VdW Energy (SD) [kJ/mol]	Electrostatics Energy (SD) [kJ/mol]	Polar Solvation (SD) [kJ/mol]	Apolar Solvation (SD) [kJ/mol]	Total Binding Energy (SD) [kJ/mol]
Epalr estat	−173.315 (±19.093)	−47.972 (±9.748)	102.526 (±22.381)	−15.994 (±1.212)	−134.755 (±19.086)
Astax anthin	−244.529 (±20.977)	−54.520 (±16.280)	140.664 (±25.181)	−27.885 (±3.490)	−186.271 (±18.571)
Astax anthin	−244.529 (±20.977)	−20.856 (±16.587)	117.821 (±18.136)	−25.044 (±2.460)	−123.557 (±19.585)

All the components of energy are representative of average values over the first 20 ns. MD simulations were calculated using the MMPBSA techniques, as shown in Table 3. Among the free energy components, van der Waals energy, electrostatics energy, and solvent accessible surface area (SASA) have a negative value of total binding energy. In contrast, polar solvation energy has positive total free binding energy. These findings supported the binding energy values obtained from the docking calculations. However, the low binding energy values obtained in MD was due to the energy contributions from solvation. However, it was observed that the contributions from Vander Waals energy were strongest compared to other energy components (Table 3). This might be a contributing factor toward the strongest binding affinity. The highest negative values of Van der Waals energy are an indication of massive contributions from hydrophobic residues.

Per residue binding energy contribution for AR with known inhibitor suggested that Trp20, Lys21, Asp43, Val47, Tyr48, Gln49, Glu51, Trp79, Phe121, Lys262 and Ala299 (Figure 5) were the major residues interacting with the epalrestat. The most favorable interacting amino acid residues were Trp20, Tyr48, Phe121, Trp79, and Val47 with binding energies of −11.6309, −9.7238, −8.3614, −4.9392, and −4.3825 kJ/mol respectively. Astaxanthin bind with AR through these amino acid residues; Trp20, Lys21, Tyr48, Trp111, Phe121, Trp219, Arg293, Arg296, Ala299, Leu300, Pro310, and Glu313 (Figure 5). Amino acid residues that showed most favorable energy contribution were given in the following sequential order Leu300 > Tyr48 > Phe121> Ala299 >Trp20 each with binding of −12.784, −8.432, −8.321, −7.2028 and −6.8900 kJ/mol respectively. In AR-zeaxanthin complex interaction, amino acid residues that interact favorably with AR were Phe122, Trp79, Pro23, Pro24, and Trp111 with binding energies of −6.978, −6.866, −4.982, −4.687, and −4.214 kJ/mol respectively. Based on per residues energy analysis, it is clearly observed that astaxanthin possesses the strongest binding energy. This could probably be due to the strong, attractive electrostatic energy contribution by Leu300. Further, *in vitro* studies are however needed to ascertain our findings.

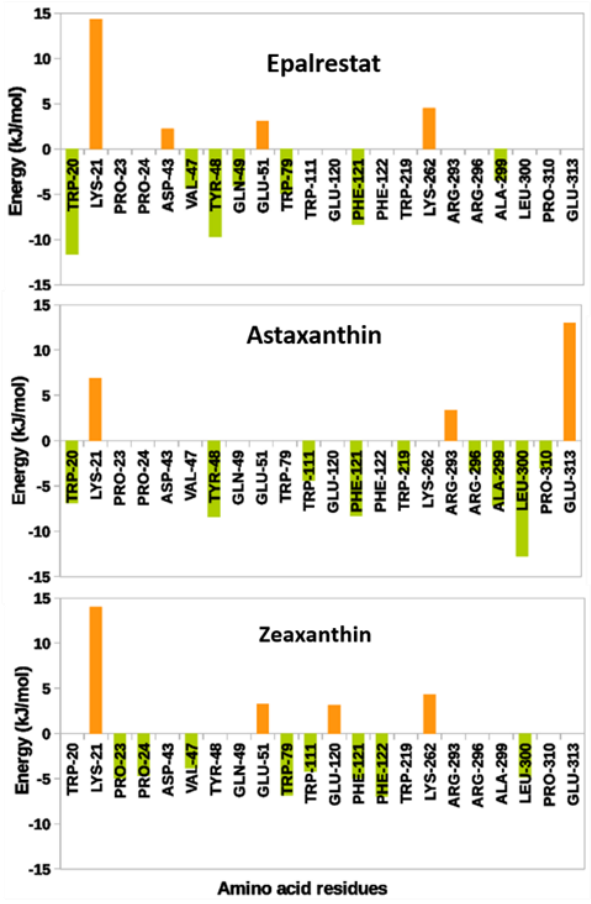

Figure 5. Per residue energy contributions (in kJ/mol) of all the inhibitors, orange bars represent amino acids with unfavorable binding energy. In contrast, light green bars represent amino acids with favorable binding energy.

4. Conclusions

The structure-function relationship is very fundamental to the understanding of physiological processes. Biological function is based on molecular interactions within or between macromolecular structures. In our study, molecular docking and MD simulation techniques demonstrate that astaxanthin could efficiently interact and inhibit aldose reductase better than epalrestat. This inhibition might be due to the strongest energy contributions seen in Leu300 but not found in the known inhibitor. By implication, this natural molecule could serve as a safe alternative and a promising drug candidate for treating diabetes-induced cataract and other chronic effects associated with diabetes rather than using the chemically synthesized epalrestat.

Acknowledgments

The second author was financially supported by Rajamangala University of Technology Phra Nakhon (RMUTP) research scholarship.

Conflicts of interest

The authors declare that there are no conflicts of interest related to this study.

References

1. Badria FA, Elimam DM, Elabshihy MSI, et al. Aldose reductase inhibitors from nature: A new hope for treatment of cataract.
2. Chethan S, Dharmesh SM, Malleshi NG (2008) Inhibition of aldose reductase from cataracted eye lenses by finger millet (Eleusine coracana) polyphenols. *Bioorgan Med Chem* 16: 10085–10090.
3. Kyselova Z, Stefek M, Bauer V (2004) Pharmacological prevention of diabetic cataract. *J Diabetes Complicat* 18: 129–140.
4. Wang Z, Ling B, Zhang R, et al. (2009) Docking and molecular dynamics studies toward the binding of new natural phenolic marine inhibitors and aldose reductase. *J Mol Graph Model* 28: 162–169.
5. Ribaya-Mercado JD, Blumberg JB (2004) Lutein and zeaxanthin and their potential roles in disease prevention. *J Am Coll Nutr* 23: 567S–587S.
6. Yu B, Wang J, Suter PM, et al. (2012) Spirulina is an effective dietary source of zeaxanthin to humans. *Brit J Nutr* 108: 611–619.
7. Ekpe L, Inaku K, Ekpe V (2018) Antioxidant effects of astaxanthin in various diseases—A review. *J Mol Pathophysiol* 7: 1–6.
8. Yang M, Chen Y, Zhao T, et al. (2020) Effect of astaxanthin on metabolic cataract in rats with type 1 diabetes mellitus. *Exp Mol Pathol* 113: 104372.
9. Ishikawa S, Hashizume K, Nishigori H, et al. (2015) Effect of astaxanthin on cataract formation induced by glucocorticoids in the chick embryo. *Curr Eye Res* 40: 535–540.
10. Benlarbi-Ben Khedher M, Hajri K, Dellaa A, et al. (2019) Astaxanthin inhibits aldose reductase activity in Psammomys obesus, a model of type 2 diabetes and diabetic retinopathy. *Food Sci Nutr* 7: 3979–3985.
11. Du X, Li Y, Xia YL, et al. (2016) Insights into protein–ligand interactions: mechanisms, models, and methods. *Int J Mol Sci* 17: 144.
12. Olsson TS, Williams MA, Pitt WR, et al. (2008) The thermodynamics of protein–ligand interaction and solvation: insights for ligand design. *J Mol Biol* 384: 1002–1017.
13. Bronowska AK (2011) Thermodynamics of ligand-protein interactions: implications for molecular design. *Thermodynamics-Interaction Studies-Solids, Liquids and Gases*: IntechOpen.
14. Martin SF, Clements JH (2013) Correlating structure and energetics in protein-ligand interactions: paradigms and paradoxes. *Annu Rev Biochem* 82: 267–293.
15. Martis EAF, Coutinho EC (2019) Free energy-based methods to understand drug resistance mutations. *Structural Bioinformatics: Applications in Preclinical Drug Discovery Process*: Springer, 1–24.
16. Kim S, Thiessen PA, Bolton EE, et al. (2016) PubChem substance and compound databases. *Nucleic Acids Res* 44: D1202–D1213.
17. Hanwell MD, Curtis DE, Lonie DC, et al. (2012) Avogadro: an advanced semantic chemical editor, visualization, and analysis platform. *J Cheminformatics* 4: 17.

18. Bohren KM, Brownlee JM, Milne AC, et al. (2005) The structure of Apo R268A human aldose reductase: hinges and latches that control the kinetic mechanism. *(BBA)-Proteins Proteom* 1748: 201–212.
19. Morris GM, Huey R, Lindstrom W, et al. (2009) AutoDock4 and AutoDockTools4: Automated docking with selective receptor flexibility. *J Comput Chem* 30: 2785–2791.
20. Laskowski RA, Swindells MB (2011) LigPlot+: multiple ligand-protein interaction diagrams for drug discovery. *J Chem Inf Model* 51: 2778–2786.
21. Abraham MJ, Murtola T, Schulz R, et al. (2015) GROMACS: High performance molecular simulations through multi-level parallelism from laptops to supercomputers. *SoftwareX* 1: 19–25.
22. Schmid N, Eichenberger AP, Choutko A, et al. (2011) Definition and testing of the GROMOS force-field versions 54A7 and 54B7. *Eur Biophys J* 40: 843.
23. Mark P, Nilsson L (2001) Structure and dynamics of the TIP3P, SPC, and SPC/E water models at 298 K. *J Phys Chem A* 105: 9954–9960.
24. Stroet M, Caron B, Visscher KM, et al. (2018) Automated topology builder version 3.0: Prediction of solvation free enthalpies in water and hexane. *J Chem Theory Comput* 14: 5834–5845.
25. Darden T, York D, Pedersen L (1993) Particle mesh Ewald: An N·log(N) method for Ewald sums in large systems. *J Chem Phys* 98: 10089–10092.
26. Berendsen HJC, Postma JPM, van Gunsteren WF, et al. (1984) Molecular dynamics with coupling to an external bath. *J Chem Phys* 81: 3684–3690.
27. Martoňák R, Laio A, Parrinello M (2003) Predicting crystal structures: the Parrinello-Rahman method revisited. *Phys Rev Lett* 90: 075503.
28. Humphrey W, Dalke A, Schulten K (1996) VMD: Visual molecular dynamics. *J Mol Graph* 14: 33–38.
29. Kumari R, Kumar R, Consortium OSDD, et al. (2014) g_mmpbsa—A GROMACS tool for high-throughput MM-PBSA calculations. *J Chem Inf Model* 54: 1951–1962.
30. Duan LL, Feng GQ, Zhang QG (2016) Large-scale molecular dynamics simulation: Effect of polarization on thrombin-ligand binding energy. *Sci Rep* 6: 31488.
31. Ren J, Yuan X, Li J, et al. (2020) Assessing the performance of the g_mmpbsa tools to simulate the inhibition of oseltamivir to influenza virus neuraminidase by molecular mechanics Poisson–Boltzmann surface area methods. *J Chin Chem Soc* 67: 46–53.
32. Lee HS, Jo S, Lim H-S, et al. (2012) Application of binding free energy calculations to prediction of binding modes and affinities of MDM2 and MDMX inhibitors. *J Chem Inf Model* 52: 1821–1832.
33. Umamaheswari M, Aji C, Kuppusamy A, et al. (2012) In silico docking studies of aldose reductase inhibitory activity of selected flavonoids. *Int J Drug Dev Res* 4: 328–334.
34. Khan S, Bhardwaj T, Somvanshi P, et al. (2018) Inhibition of C298S mutant of human aldose reductase for antidiabetic applications: Evidence from in silico elementary mode analysis of biological network model. *J Cell Biochem* 119: 6961–6973.
35. Naeem S, Hylands P, Barlow D (2013) Docking studies of chlorogenic acid against aldose redutcase by using molgro virtual Docker software. *J Appl Pharm Sci* 3: 13–20.
36. Padmaja S, MP, Raju TN (2016) Molecular docking studies of Hemidesmus indicus plant derived compounds as aldose reductase inhibitors. *Int J Pharm Sci Rev Res* 37: 92–95.

AIMS Press